RSC Advances

PAPER

View Article Online
View Journal | View Issue

Cite this: *RSC Adv.*, 2020, **10**, 8255

Catalytic activity of porous carbon nitride regulated by polyoxometalates under visible light†

Shuge Tang,[a] Zhuang Liu,[a] Fengpan Ma,[a] Guilong Cao,[a] Jingkuan Wang,[b] Wei Chen,[a] Xiaojia Feng*[a] and Yongfa Zhu*[c]

Received 13th December 2019
Accepted 21st January 2020

DOI: 10.1039/c9ra10441k

rsc.li/rsc-advances

A series of porous carbon nitrides modified by different polyoxometalates (POMs) were prepared by the ultrasonic method. POMs were assembled on the surface of mpg-C_3N_4 *via* electrostatic attraction. The catalyst has visible light degradation activity for phenol ($\lambda > 420$ nm). mpg-C_3N_4 modified by $H_4SiW_{12}O_{40}$ with a mass ratio of 1 : 5 showed the highest catalytic activity, which was 3.5 times higher than that of mpg-C_3N_4. As an electron acceptor, polyoxometalate can capture the photoelectron of C_3N_4, which can promote the separation of photocharge and improve the photocatalytic activity. ESR also confirmed that the superoxide radicals play a major role in degradation. The results show that the charge separation efficiency and catalytic activity can be enhanced by polyacids.

Introduction

Graphitic carbon nitride (g-C_3N_4) is the first visible light response material discovered in the field of photocatalysis. Its crystal structure is very simple. The valence band is made up of N 2p orbitals, and the conduction band is made up of C 2p orbitals. Due to its unique electronic structure, suitable bandgap width, high thermal and chemical stability, environmental friendliness, low cost, *etc.*, it has wide application prospects in the fields of catalysis, environmental governance, sensors, drug carriers, and other fields.[1–3] Although carbon nitride (g-C_3N_4) has attracted considerable attention in the field of photocatalysis, pure g-C_3N_4 has many disadvantages: (1) due to its special lamellar structure, the photocatalytic degradation efficiency of pollutants is not high; (2) the specific surface area is small; and (3) the visible light utilization is less.[4] These shortcomings limit its large-scale applications in environmental purification. Therefore, it is necessary to modify C_3N_4 by extending the visible light absorption of g-C_3N_4 and reducing the photogenerated electron–hole recombination rate.[4–6] Various C_3N_4/semiconductor complexes have been reported, including C_3N_4/TiO_2, C_3N_4/ZnO, C_3N_4/CdS, and C_3N_4/precious metal, all of which significantly improve the photocatalytic activity of C_3N_4.[7,8]

The pore structure of a catalyst has a certain influence on its performance. Porous g-C_3N_4 (mpg-C_3N_4) has a larger specific surface area than pure g-C_3N_4. Apart from this, it has abundant catalytic active sites and also exhibits the crystallization with open hole, which is conducive to the diffusion of the mpg-C_3N_4 nanostructure, improving the ability to capture light and helping other photocatalytic materials to grow on its surface. Therefore, on the basis of mpg-C_3N_4, the catalytic effect of g-C_3N_4 can be greatly improved by the compound method. It is the most common way to improve the photocatalytic activity to improve the poor separation efficiency of carriers by means of heteroatom binding, semiconductor composite, and supporting Pt, Au, and other precious metal ions.[9–11]

Polyoxometalates (POMs) after the electronic reversible redox process become a more complete structure, which means that more acids can be used for electronic "shallow well" capture and storage; at the same time, under the condition of appropriate release, they also exhibit electronic capture and have strong electronic storage capacity, due to which more acids as electron acceptors can improve the semiconductor optical carrier separation.[12–15] Using this property, it is expected to realize the effective separation of semiconductor photocarriers and improve the photocatalytic efficiency. Professor Zhangguangjin loaded multi-walled carbon nanotubes with Au nanoparticles wrapped in an acid (Au NPs@POM-CNT).[16] The $H_3PW_{12}O_{40}$-doped C_3N_4 nanotubes prepared by Professor Luo Shenglian exhibit excellent visible light degradation of methyl orange and organic pollutants.[17]

The catalytic mechanism shows that the photoelectrons generated by C_3N_4 are transferred to the LUMO orbital of PW_{12} under the excitation of visible light, and the photogenerated holes stay in the valence band of C_3N_4. The transferred electrons and holes generate free radicals with high redox activity and react with the adsorbed substrate molecules, respectively.[18–20]

In this study, a series of porous g-C_3N_4 complexes were designed and synthesized using POMs, and a variety of acids

[a]*Department of Science, Shenyang Agriculture University, China. E-mail: 2013500007@syau.edu.cn; zhuyf@mail.tsinghua.edu.cn*

[b]*Department of Land Environment, Shenyang Agriculture University, China*

[c]*Department of Chemisty, Tsinghua University, China*

† Electronic supplementary information (ESI) available. See DOI: 10.1039/c9ra10441k

were used to regulate the photocatalytic activity of C_3N_4. The polyacids include $H_3PW_{12}O_{40}$, $H_3PMo_{12}O_{40}$, $H_4SiW_{12}O_{40}$, and $H_4SiMo_{12}O_{40}$. The regulation of the photocatalytic activity of C_3N_4 without polyacids was discussed.

Results and discussion

Controllable construction of C_3N_4-POM composite structure

Because mpg-C_3N_4 has a large volume and layered structure, in order to make full contact between the polyacid and mpg-C_3N_4, ultrasound was first used to peel it off. The acid was then combined with the stripped mpg-C_3N_4 through electrostatic attraction and hydrogen bonding. In order to enhance the bonding of polyoxoanions with C_3N_4, the composite was annealed at 200 °C. POM-modified C_3N_4 was successfully prepared by the above-mentioned steps.

The XRD results shown in Fig. 1a indicate that mpg-C_3N_4 has two characteristic absorption peaks at 13.1° and 27.0°, corresponding to the C_3N_4 (JCPD-1526) crystal planes of (100) and (002). The absorption peak at 27.3° corresponds to the accumulation direction between the (002) crystal plane of g-C_3N_4 and the CN aromatic plane. There is no characteristic diffraction peak of the polyacid, indicating that the compound amount is very small and the crystallinity of polyanions is poor. The diffraction peak at 27.3° corresponds to the (002) crystal plane of the mpg-C_3N_4 thin layer.[21] After compounding with polyanions, the peaks shift slightly. This is because the electrostatic attraction and hydrogen bonding between multiple acids and mpg-C_3N_4 reduces the spacing between the layers of C_3N_4, indicating that multiple acids have compounded to the surface of C_3N_4. Polyacids can act as electron acceptors to capture the photogenerated electrons of C_3N_4, thus improving the photocatalytic activity of C_3N_4.

The spectral absorption properties of the complex were determined by a UV-vis diffuse reflectometer (DRS), as shown in Fig. 1b. The absorption band edge of both mpg-C_3N_4 and g-C_3N_4 was 450 nm, which was consistent with the band width of g-C_3N_4 reported in the literature (about 2.7 eV). The absorption band edges of SiW_{12} and PW_{12} were at 400 nm and 420 nm, and the absorption band edges of $SiMo_{12}$ and PMo_{12} were at 500 nm and 550 nm, respectively. The optical absorption range of the products of SiW_{12}, PW_{12}, $SiMo_{12}$, and mpg-C_3N_4 in the visible region was the same as that of mpg-C_3N_4, indicating that there was no effect on the spectral absorption of C_3N_4. The absorption intensity of PMo_{12}/C_3N_4 in the visible region was slightly enhanced.

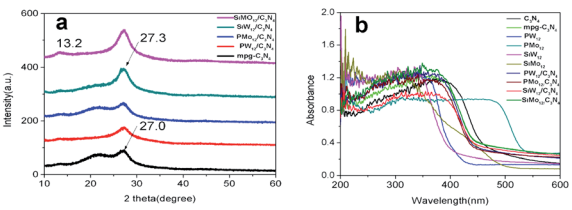

Fig. 1 (a) The XRD patterns of C_3N_4 and POM/C_3N_4; (b) the UV-vis spectra of C_3N_4, POM and POM/C_3N_4.

The morphology of SiW_{12}/C_3N_4 was characterized by scanning electron microscopy (SEM) and high-resolution transmission electron microscopy (HRTEM). The SEM (Fig. 3) and TEM (Fig. S2†) images show that the prepared CN has a porous structure. In Fig. 2, we can observe that many polyacid particles are distributed on the surface of C_3N_4, and their size is 1 nm. The SEM images (Fig. 3 and S3†) show that g-C_3N_4 has a distinct layered structure with a smooth surface and no other components; pores of different sizes are distributed on the surface of mpg-C_3N_4. The EDAX map (Fig. S3†) and the related element distribution indicated that C, Si, and W existed in the complex, and the polyacid mass fraction in SiW_{12}/C_3N_4-3 was about 2%. The XPS results also showed that the polyacid successfully

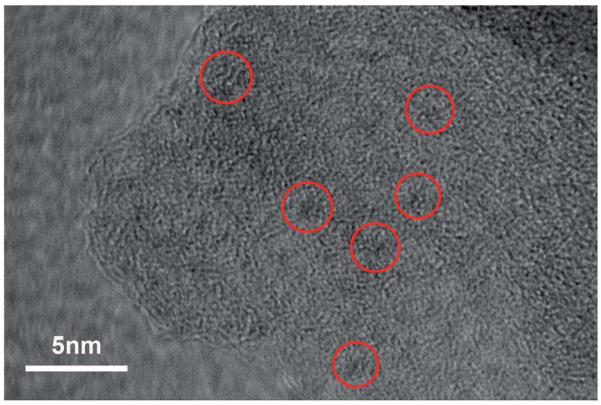

Fig. 2 HRTEM image of SiW_{12}/C_3N_4-3.

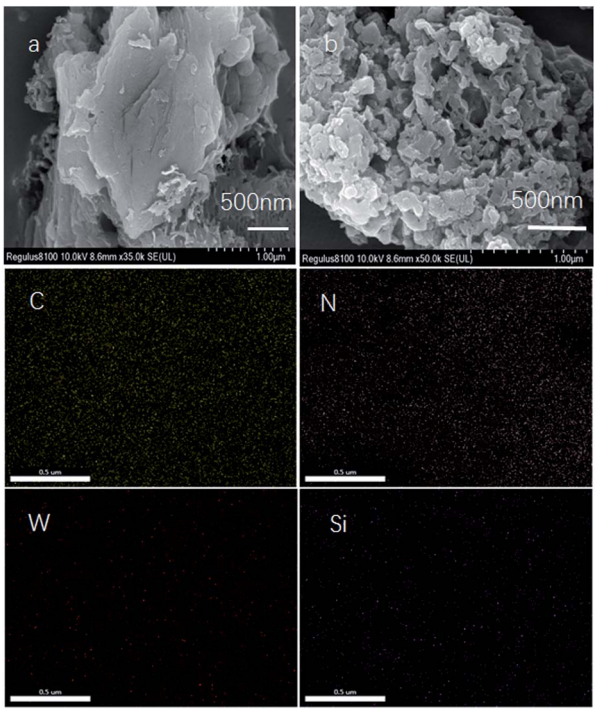

Fig. 3 SEM images of (a) g-C_3N_4 and (b) mpg-C_3N_4.

modified the surface of C_3N_4. The BET adsorption curve (Fig. S4†) shows that there is a hysteresis loop. Combined with the SEM images, we can observe that there are holes of about 100 nm; thus, the materials are basically between macroporous and mesoporous ones, with a specific surface area of 41.899 $m^2\ g^{-1}$.

Catalytic activity by the composite structure

The phenol degradation under visible light was evaluated to reveal the photocatalytic activity of the composite structure. Blank experiments showed that phenol basically did not degrade without the catalyst. Under visible light irradiation, the activity of POMs/mpg-C_3N_4 was better than that of bulk g-C_3N_4 and mpg-C_3N_4. When only g-C_3N_4 was used as the catalyst, the phenol degradation was about 13.4%, that for mpg-C_3N_4 was 26.2%, and the degradation efficiency of POMs/mpg-C_3N_4 improved, indicating that the introduction of a polyacid improved the photocatalytic activity. In a composite structure, the addition of multiple acids reduces the composite center of carriers and accelerates the separation of photogenerated electrons and holes. The order of the catalytic efficiency of different polyacids is SiW_{12}/C_3N_4 > PW_{12}/C_3N_4 > PMo_{12}/C_3N_4 > $SiMo_{12}/C_3N_4$. SiW_{12}/C_3N_4 has the best activity, which is 6.8 times that of g-C_3N_4 and 3.5 times that of mpg-C_3N_4. With the increase in the SiW_{12} content, the activity of the complexes also increased but when the ratio of SiW_{12} increased to 1 : 5, the activity was the highest, and the catalytic activity of SiW_{12} no longer increased. It is known that polymetallic oxalate is an excellent electron capture center, which can speed up the separation of photogenerated carriers with an appropriate concentration. If too many polyanions are loaded, it will become the recombination center, which reduces the photocatalytic performance of the composite. Therefore, the catalytic activity of SiW_{12}/C_3N_4-4 and SiW_{12}/C_3N_4-5 decreased. Cyclic experiments were conducted to investigate the stability of the complex using SiW_{12}/C_3N_4-3 as an example. It was observed that after three cycles, the degradation rates of phenol were 90.3%, 82.4%, and 70.2%. The catalytic activity of g-C_3N_4 and mpg-C_3N_4 decreased by 44.5% and 58.5%, respectively, after three cycles. The photodegradation activity after the two subsequent cycling tests did not decrease significantly compared with that for the first test, indicating that SiW_{12}/C_3N_4 had good stability (Fig. 4 and 5).

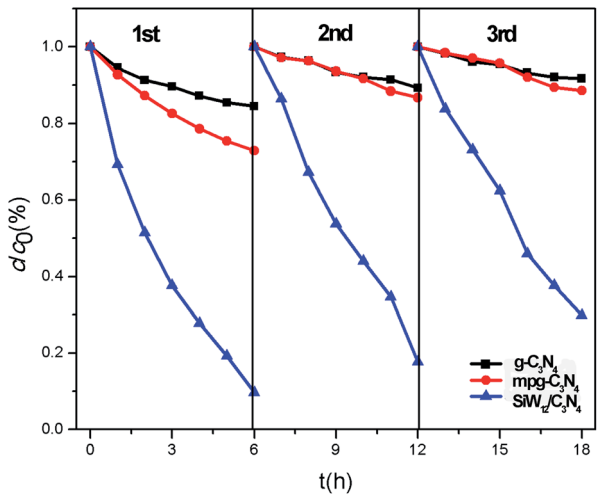

Fig. 4 Recycle experiment on the SiW_{12}/C_3N_4-3 activity for degradation of phenol under visible light.

Mechanism of enhancing the photocatalytic activity of the composite structure

(1) Photoluminescence spectroscopy and electrochemical impedance spectroscopy. The separation, migration, and recombination of photocarriers in the compound photocatalyst were studied by the PL technique. As shown in Fig. 6, mpg-C_3N_4 exhibits the strongest intensity in the fluorescence emission spectrum at 460 nm; as the modified SiW_{12} content increases, the fluorescence emission intensity of the complex decreases gradually, suggesting that SiW_{12} as electronic photoproduction by physical capture C_3N_4, which accelerates the separation of the carriers and reduces the recombination probability of the photogenerated electrons and holes. The fluorescence emission intensities of SiW_{12}/C_3N_4-3, $SiMo_{12}/C_3N_4$, PW_{12}/C_3N_4 and

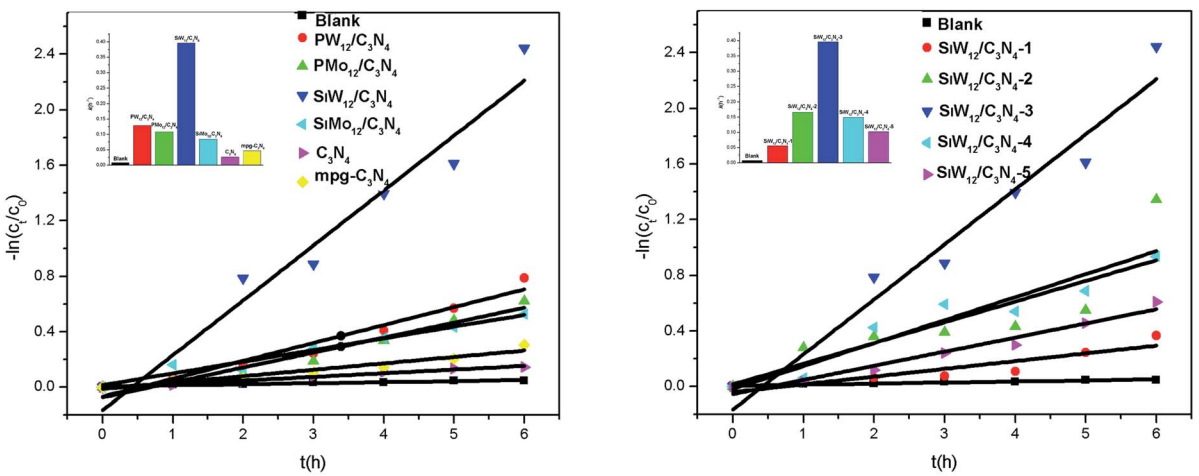

Fig. 5 Photocatalytic activity of phenol under visible light.

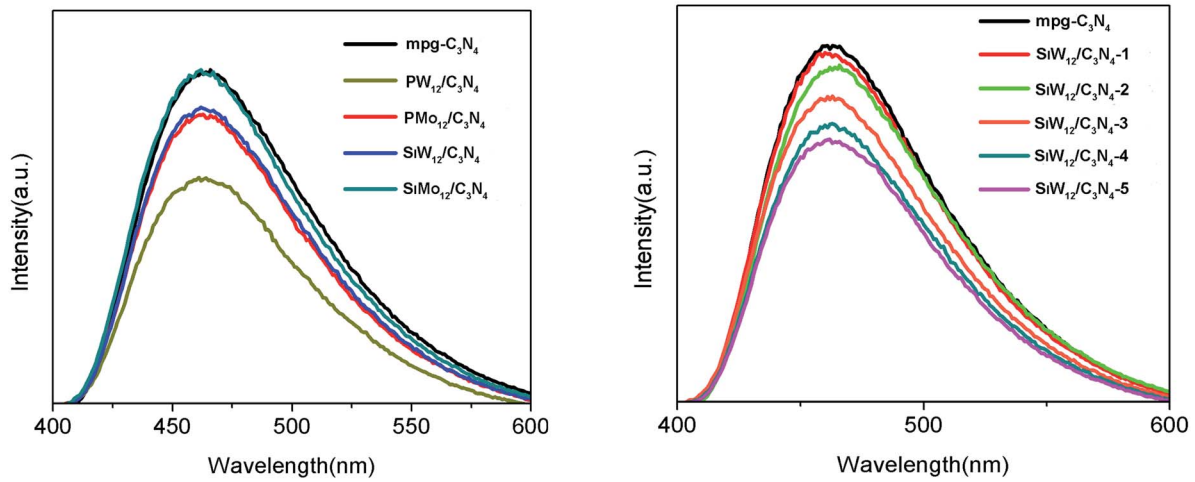

Fig. 6 The photoluminescence (PL) spectra of POM/C_3N_4.

PMo_{12}/C_3N_4 are all lower than that of mpg-C_3N_4, indicating that these polyacids can act as electron receptors to capture the photogenerated electrons of C_3N_4 and reduce their fluorescence intensity. $SiMo_{12}/C_3N_4$ > SiW_{12}/C_3N_4 > PMo_{12}/C_3N_4 > PW_{12}/C_3N_4, indicating that the ability to capture electrons for the four polyacids is from high to low: PW_{12} > PMo_{12} > SiW_{12} > $SiMo_{12}$. In the composite structure, the addition of multiple acids reduces the composite center of the carriers and accelerates the separation of the photogenerated electrons and holes. SiW_{12}/C_3N_4 > PMo_{12}/C_3N_4 > PW_{12}/C_3N_4, indicating that the ability to capture electrons for the four polyacids ranges from high to low: PW_{12} > PMo_{12} > SiW_{12} > $SiMo_{12}$. In the composite structure, the addition of multiple acids reduces the composite center of carriers and accelerates the separation of the photogenerated electrons and holes.

The surface composition and the chemical state of the complex were characterized by XPS. C, N, O, Si, and W exist in SiW_{12}/C_3N_4-3. Fig. 7 shows that the binding energies of C 1s are 288.3 and 284.8 eV. The peak at 288.3 eV corresponds to the sp^2 carbon (C–N=C), and the peak at 284.8 eV corresponds to the graphitized carbon. The peak at 399 eV corresponds to ternary N–$(C)_3$ or H–N–$(C)_2$, and the peak at 400.1 eV is assigned to the aromatic ring. The O1s spectrum can be divided into three peaks at 530.2 eV, 530.9 eV, and 532 eV. The binding energy of 101.8 eV corresponds to the Si–O bond, which is consistent with the standard value of Si 2p. The W 4f spectrum shows that the

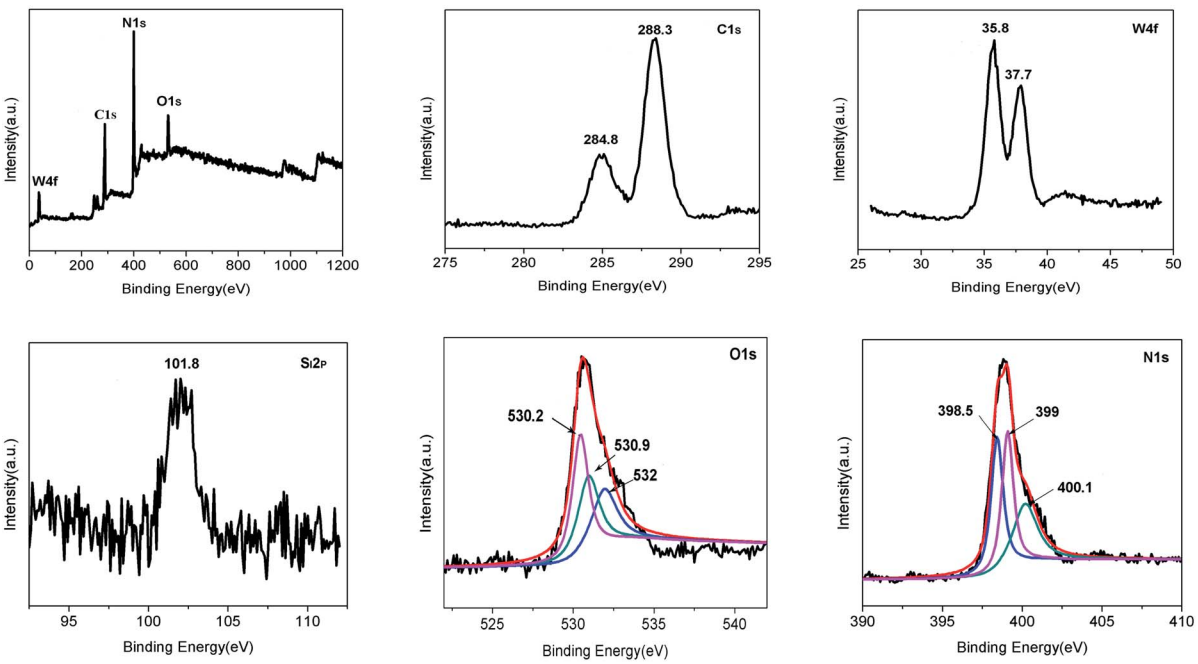

Fig. 7 The XPS spectra of SiW_{12}/C_3N_4-3.

binding energies are 35.8 eV and 37.7 eV, indicating that the W element is at the highest valence, *i.e.*, W^{6+}, which is consistent with the previous report.[22]

(2) Photocatalytic mechanism. The interface charge separation efficiency was studied by electrochemical impedance spectroscopy (EIS). As can be seen from Fig. 8a, the arc radius in the $SiMo_{12}/C_3N_4$ impedance spectrum is significantly smaller than that for other catalysts with multiple acids and C_3N_4 composites and also smaller than that of pure C_3N_4 with light irradiation. The results showed that the composite catalyst could increase the photocatalytic activity and increase the separation and transfer of photocatalytic active charge at the interface.[23]

A free radical capture experiment was used to study the catalytic mechanism. The free radical capture agents included triethanolamine (TEOA), isopropanol (IPA), and *p*-benzoquinone (BQ), which were used to capture the photosynthetic holes (h^+), hydroxyl radicals ($^{\cdot}OH$), and superoxide radicals ($^{\cdot}O_2^-$) of the reactive species, respectively. The concentrations of TEOA, IPA, and BQ were 1.0 mmol L^{-1}, 10 mmol L^{-1} and 1.0 mmol L^{-1}, respectively. Before the photocatalytic test, the capture agent was added to the phenol solution, and the more serious the degradation rate, the more important the relative species captured by the capture agent for the photocatalytic process. The addition of BQ can inhibit the photocatalytic reaction, while isopropanol and triethanolamine have almost no effect on phenol degradation, indicating that superoxide free radicals ($^{\cdot}O_2^-$) were the main active species in the photocatalytic degradation reaction (Fig. S5†).

In order to further elucidate the mechanism of photocatalytic degradation, ESR was used to detect the main oxidizing substances during the photocatalytic degradation. As shown in Fig. 8b, there was no obvious hydroxyl superoxide radical ($\cdot O_2^-$) formation in the DMSO solution without light. After exposure to visible light, both C_3N_4 and $SiMo_{12}/C_3N_4$ produce $\cdot OOH$ ($\cdot O_2^-$ receiving proton H^+ in DMSO generate $\cdot OOH$), $H_4SiW_{12}O_{40}$ mainly produces hydrogen radical after illumination ($\cdot H$). Fig. 8c showed that under the light condition, both C_3N_4 and $SiMo_{12}/C_3N_4$ produced $\cdot OH$ in the aqueous solution, while $H_4SiW_{12}O_{40}$ had no $\cdot OH$ signal peak. Combined with the free radical capture experiment, the results show that the superoxide radical ($^{\cdot}O_2^-$) was the main active material in the photocatalytic degradation.[24,25]

Experimental

Preparation

(1) mpg-C_3N_4. First, 300 nm $CaCO_3$ was placed at 550 °C for 12 h; the surface organic layer was removed and then, 0.5 g cyanamide (DCDA) and 2 g 300 nm $CaCO_3$ were mixed according to the mass ratio of 1 : 4. Subsequently, 30 mL water was added and the dry powder was concentrated at 100 °C; then, it was kept at 3.1 °C min^{-1} to 400 °C in nitrogen for 2 hours, 1 mol L^{-1} hydrochloric acid for 2 hours to remove $CaCO_3$, and at 4.4 °C min^{-1} to 400 °C until 550 °C for 2 hours.

(2) $H_4SiMo_{12}O_{40}$. We added 37 mL concentrated HNO_3 to 120 mL 1 M Na_2MoO_4 solution and then, 50 mL 0.2 M Na_2SiO_3 solution was added dropwise to it. Next, we added 40 mL concentrated HCl, cooled to room temperature, and extracted with 80 mL ether, followed by the release of the ether layer. Subsequently, 40 mL water was added, and it was then dried in vacuum to obtain yellow crystals.

(3) POMs/mpg-C_3N_4. First, 0.5 g mpg-C_3N_4 powder was added into 20 mL methanol, and the lamellar mpg-C_3N_4 was evenly dispersed by ultrasound for 14 h. Different polyacids, namely, $H_3PW_{12}O_{40}\cdot xH_2O$, $H_3PMo_{12}O_{40}\cdot xH_2O$, $H_4SiW_{12}O_{40}\cdot 26H_2O$, and $H_4SiMo_{12}O_{40}$ with a certain mass were dissolved in 10 mL methanol and were added to the mpg-C_3N_4 suspension for 4 h ultrasonication. Subsequently, it was washed with methanol, dried at 60 °C, and then kept at 200 °C for 4 h in a muffle furnace. The products were named as PW_{12}/C_3N_4, PMo_{12}/C_3N_4, SiW_{12}/C_3N_4 and $SiMo_{12}/C_3N_4$. $H_4SiW_{12}O_{40}\cdot 26H_2O$ and mpg-C_3N_4 were prepared according to different mass ratios of 1 : 50, 1 : 10, 1 : 5, 3 : 10, and 6 : 10. The products were named as SiW_{12}/C_3N_4-1, SiW_{12}/C_3N_4-2, SiW_{12}/C_3N_4-3, SiW_{12}/C_3N_4-4, and SiW_{12}/C_3N_4-5.

Characterizations

An HT7700 TEM transmission electron microscope, HITACHI Regulus8100 scanning electron microscope and JEM-2011F high-resolution electron microscope (HRTEM) were used to characterize the product morphology. UV-3010 (Shimadzu) UV-

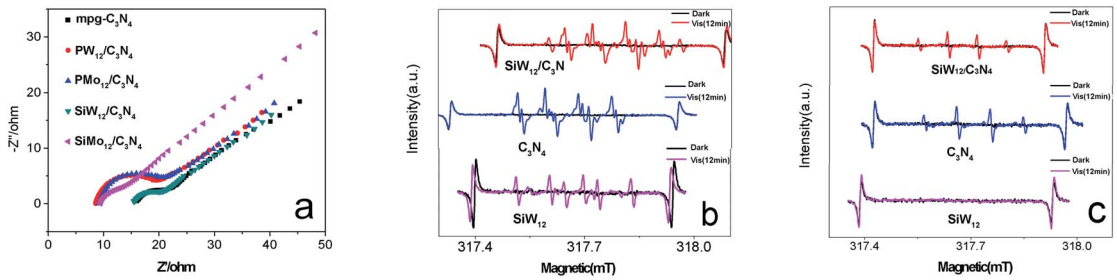

Fig. 8 (a) EIS Nynquist plot under visible light irradiation (λ_{vis} > 20 nm) [Na_2SO_4 = 0.1 M]. (b) ESR of superoxide radical test in DMSO (100 mM) as radical trapper under visible light irradiation (λ_{vis} > 420 nm). (c) ESR of hydroxyl radical test in an aqueous solution under visible light (λ_{vis} > 420 nm).

visible solid diffuse reflection (DRS) was used to characterize the spectral properties of the products. The XPS data of the product were characterized by the PHI Quantera SXMTM system. The fluorescence spectra were measured with a Varian Cary Eclipse500 fluorescence photometer, and the excitation wavelength was 320 nm. The photocurrents were measured on the CHI 660B electrochemical system. The active species of phenol degradation can be detected by ESR (JEOL JES-FA200 ESR Spectrometer) using dimethyl sulfoxide (DMSO) as a free radical trapping agent.

Photocatalytic experiments

The 350 W Xe lamp was used as the visible light source, the 420 nm filter was used to filter the ultraviolet light, and the XPA-7 photochemical reaction instrument was used. Before illumination, 50 mg catalyst was mixed with 50 mL 1×10^{-5} mol L^{-1} phenol solution, and the dark equilibrium was maintained for 1 h, thereby reaching the adsorption–desorption equilibrium on the catalyst surface. After light exposure, the reaction solution was taken at an interval of 1 h. The concentration of phenol was analysed by Shimadzu LC-20A high-performance liquid chromatography (HPLC) with a Venusil XBP-C18 and a UV detector at 270 nm. The mobile phase consisted of methanol and water (volume ratio: 55/45) at a flow rate of 1 mL min^{-1}.

A series of mpg-C_3N_4 complexes modified by polyacids (POMs = $H_3PW_{12}O_{40}$, $H_3PMo_{12}O_{40}$, $H_4SiW_{12}O_{40}$, and $H_4SiMo_{12}O_{40}$) were prepared. The results of XRD, TEM, XPS, and EDAX confirmed that a small amount of a polyacid was modified on the surface of mpg-C_3N_4 by electrostatic interaction and hydrogen bonding. Photocatalysis demonstrated the complex's high visible light degradation of phenol ($\lambda > 420$ nm). The content and type of a polyacid can regulate the photocatalytic activity of the product. The 1 : 5 SiW_{12}-modified mpg-C_3N_4 had the highest catalytic activity. The catalytic mechanism indicates that the polyacid as an electron acceptor can capture the photogenerated electrons of C_3N_4 and promote the separation of photogenerated carriers, leading to improved photocatalytic activity. This work has great significance for the study of polyacids to improve the photocatalytic activity of semiconductors.

Conflicts of interest

There are no conflicts to declare.

Acknowledgements

This work was partly supported by National Nature Science Foundation of China (21401131).

Notes and references

1 J. Wang, C. Zhang, Y. Shen and Z. Zhou, *J. Mater. Chem. A*, 2015, **3**, 5126.
2 Y. Y. Wang, W. J. Yang and X. J. Chen, *Appl. Catal., B*, 2018, **220**, 337.
3 Y. Y. Wang, W. J. Jiang and W. J. Luo, *Appl. Catal., B*, 2018, **237**, 633.
4 J. S. Zhang, X. F. Chen, K. Takanabe, K. Maeda, K. Domen, J. D. Epping, X. Z. Fu, M. Antonietti and X. C. Wang, *Angew. Chem., Int. Ed.*, 2010, **49**, 441.
5 J. S. Zhang, J. H. Sun, K. Maeda, K. Domen, P. Liu, M. Antonietti, X. Z. Fu and X. C. Wang, *Energy Environ. Sci.*, 2011, **4**, 675–678.
6 K. Ariga, H. Ito, J. P. Hill and H. Tsukube, *Chem. Soc. Rev.*, 2012, **41**, 5800.
7 C. C. Chen, W. H. Ma and J. C. Zhao, *Chem. Soc. Rev.*, 2010, **39**, 4206.
8 C. H. Li, F. Wang and J. C. Yu, *Energy Environ. Sci.*, 2011, **4**, 100.
9 X. C. Wang, K. Maeda, X. F. Chen, K. Takanabe, K. Domen, Y. D. Hou, X. Z. Fu and M. Antonietti, *J. Am. Chem. Soc.*, 2009, **131**, 1680.
10 S. C. Yan, Z. S. Li and Z. G. Zou, *Langmuir*, 2009, **25**, 10397.
11 Y. W. Zhang, J. H. Liu, G. Wu and W. Chen, *Nanoscale*, 2012, **4**, 5300.
12 G. G. Zhang, J. S. Zhang, M. W. Zhang and X. C. Wang, *J. Mater. Chem.*, 2012, **22**, 8083–8091.
13 G. Yan, H. F. Shi, H. Q. Tan, W. B. Zhu, Y. H. Wang, H. Y. Zang and Y. G. Li, *Dalton Trans.*, 2016, **45**, 13944.
14 T. Tachikawa, S. Tojo, M. Fujitsuka and T. Majima, *Chem.–Eur. J.*, 2006, **12**, 3124.
15 X. F. Lu, Q. L. Wang and D. L. Cui, *J. Mater. Sci. Technol.*, 2010, **26**, 925.
16 G. G. Zhang, J. S. Zhang, M. W. Zhang and X. C. Wang, *J. Mater. Chem.*, 2012, **22**, 8083.
17 X. M. Liu, K. X. Li, L. S. Yan, Z. X. Zeng, S. L. Luo, X. B. Luo, H. Q. Guo and Y. H. Guo, *Appl. Catal. B: Environ.*, 2014, **156–157**, 141.
18 Z. P. Yan, Z. J. Sun, X. Liu, H. X. Jia and P. W. Du, *Nanoscale*, 2016, **8**, 4748.
19 K. Sridharan, E. Jang and T. J. Park, *Appl. Catal., B*, 2013, **142**, 718.
20 Y. J. Wang, R. Shi, J. Lin and Y. F. Zhu, *Energy Environ. Sci.*, 2011, **4**, 2922.
21 L. Tan, J. Xu, X. Zhang, Z. Hang, Y. Jia and S. Wang, *Appl. Surf. Sci.*, 2015, **356**, 447–453.
22 J. H. Xu, D. N. Li, Yu Chen, L. H. Tan, Bo Kou, F. S. Wan, W. Jiang and F. s. Li, *Nanomaterials*, 2017, **7**(12), 450.
23 C. L. Schmidt and M. Jansen, *J. Mater. Chem.*, 2010, **20**, 4183.
24 J. X. Sun, Y. P. Yuan, L. G. Qiu, X. Jiang, A. J. Xie, Y. H. Shen and J. F. Zhu, *Dalton Trans.*, 2012, **41**, 6756.
25 S. Samanta, S. Martha and K. Parida, *ChemCatChem*, 2014, **6**(5), 1453.

